Peridynamic Analysis of Fatigue Crack Growth in Fillet Welded Joints

Kyutack Hong, Selda Oterkus* and Erkan Oterkus

PeriDynamics Research Centre, Department of Naval Architecture, Ocean and Marine Engineering, University of Strathclyde, 100 Montrose Street, Glasgow, G4 0LZ, United Kingdom

Abstract

Fatigue assessment is one of the significant factors to be considered for estimating design life of structures and structural reliability during operation. Especially, for welded structures, high stress concentration, residual stresses, weld geometry and weld quality make the structure more vulnerable to fatigue failures. Therefore, approaches that are more effective are required for estimating fatigue performances of welded structures. Existing classical methods to predict the crack propagation under cyclic loadings have some difficulties in treating complicated patterns of crack growth. However, peridynamic theory has advantages on dealing with discontinuities. In this study, a peridynamic fatigue model, which is a bond damage model of remaining life, is validated by considering ASTM E647 standard compact tension test for the crack growth. After validating the PD model, the fatigue performance of the fillet welded joint is presented by predicting the fatigue crack growth under cyclic loading conditions.

Keywords: peridynamics; welded joints; fatigue damage; crack growth

*Corresponding Author: Selda Oterkus, Department of Naval Architecture, Ocean and Marine Engineering, University of Strathclyde. Email: selda.oterkus@strath.ac.uk.

Nomenclature

δ	Horizon δ
$H_{\mathbf{x}}$	Neighbourhood of the material point **x** within the horizon δ
ρ	Mass density field
x	Position vector field
u	Displacement vector field
t	Time
f	Pairwise force function
b	Prescribed body force density field
ξ	Relative position between material points **x** and $\mathbf{x}'$
η	Relative displacement between material points **x** and $\mathbf{x}'$
s	Bond stretch
c	Bond constant
K_B	Bulk modulus
s_0	Critical stretch
$G_{\mathbf{0}}$	Critical energy release rate
φ	Local damage
$\lambda_{(k)(j)}$	Remaining life of bond between material points k and j
N	Number of cycles
A	Peridynamic fatigue parameter
m	Peridynamic fatigue parameter
$\lambda^0_{(k)(j)}$	Remaining life at the initial condition at 0^{th} load cycle
$\varepsilon_{(k)(j)}$	Cyclic bond strain of the bond between material points k and j
$s^+_{(k)(j)}$	Maximum bond stretch
$s^-_{(k)(j)}$	Minimum bond stretch
R	Load ratio
A_1	Peridynamic fatigue parameter for crack nucleation
m_1	Peridynamic fatigue parameter for crack nucleation
ε_1	Cyclic bond strain of the bond which will break first
N_1	Number of cycles for the first bond breakage.
N_f	Number of cycles to failure
$\Delta\varepsilon$	Strain range

C_f Fatigue constant of the strain-life curve

m_f Fatigue constant of the strain-life curve

A_2 Peridynamic fatigue parameter for crack growth phase

m_2 Peridynamic fatigue parameter for crack growth phase

a Instantaneous crack length

$\bar{\varepsilon}(0)$ Cyclic strain of the bond next to crack tip

ΔK_{th} Threshold of stress intensity factor range

ΔK Stress intensity factor range

C Fatigue crack growth constant

M Fatigue crack growth constant

ΔK_{fc} Fatigue fracture toughness

ε_0 Fatigue limit

K_{max} Maximum stress intensity factor in a loading cycle

ΔK^+ Positive part of the range of the stress intensity factor in a loading cycle

γ Fatigue constant

$\varepsilon_{(k)(j)_{max}}$ Maximum cyclic bond strain

$\Delta\varepsilon_{(k)(j)}{}^+$ Positive part of the range of cyclic bond strain

1 INTRODUCTION

In recent years, large ships and offshore structures are produced by joining processes and the most commonly used method for joining processes is welding. In welded structures, however, there are some effects to make their welding zone vulnerable in fatigue failures, such as residual stresses, weld geometry and weld quality (Teng et. al., 2002; Sonsino, 2009; Barsoum and Jonsson, 2011). Particularly, many welded joints have inherently poor fatigue performance, since the crack growth can easily initiate at embedded cracks where there are high stress concentrations. Lukacz et. al. (2018) presented high cycle fatigue and fatigue crack propagation design curves for 5754-H22 and 6082-T6 aluminium alloys and their friction stir welded joints. Coughlin et. al. performed fatigue testing and analysis of aluminium welds under in-service highway bridge loading conditions. Maddox (2003) presented a review of methods and corresponding Codes and Standards for the fatigue assessment of welded aluminium alloy structures. Rozumek et. al. (2020) investigated the influence of heat treatment on the behaviour of fatigue crack growth in welded joints made of S355 under bending loading. The fatigue performance of many welded joints is typically estimated based on empirical data obtained from fatigue tests for different weld details. It requires much effort both in time and cost to establish the fatigue performance of many types of welded joints. Instead of fatigue tests, computational approaches are available to save time and cost. Traditionally, finite element method is one of the major computational methods to estimate the fatigue performance of structures.

Finite element method uses partial differential equations of classical continuum mechanics, which means there is inherent limitation of singularities when treating discontinuities, such as cracks. To overcome this limitation, cohesive zone model is introduced for tracking of dynamically growing cracks (Ortiz and Pandolfi, 1999; Nguyen et. al., 2001). However, it requires a priori knowledge of the path of crack propagation and cracks in cohesive model are mesh-dependent, which means crack propagations occur only along element boundaries. For the problem of mesh-dependency in the cohesive zone model, extended finite element method (XFEM) was introduced as an alternative to the cohesive zone model (Moes et. al., 2002; Gravoil et. al., 2002; Zi and Belytschko, 2003). The extended finite element method can treat cracks independent of mesh, but there are still difficulties to determine the direction of crack propagation in three-dimensional models and it requires additional failure criteria. On the other hand, Silling (2000) introduced Peridynamic theory, which can treat discontinuities and material failures without additional criteria for describing the crack growth. Peridynamic equations involve integral equations instead of partial derivatives. Therefore, it is

possible to accurately predict crack initiation and propagation without any special techniques. It can also predict complex crack patterns in structures. There has been a significant progress in peridynamics research especially during the last few years. Amongst these Alpay and Madenci (2013) used peridynamics to predict crack growth in fully coupled thermal and deformation fields. Vazic et. al. (2017) and Basoglu et. al. (2019) investigated the micro-crack macro-crack interactions in peridynamic framework. Bie et. al. (2020) presented implementation of dual peridynamics for brittle fracture in Abaqus software. Chen et. al. (2019) used a refined thermomechanical fully coupled peridynamic formulation to investigate concrete cracking. In another study, Dong et. al. (2020) developed an improved mesoscale damage model for quasi-brittle fracture analysis of concrete with ordinary state-based peridynamics. Huang et. al. (2019) introduced a new peridynamic model for visco-hyperelastic material deformation in different strain rates. Imachi et. al. (2019, 2020) demonstrated the capability of peridynamics in dynamic fracture analysis. Liu et. al. (2018) presented simulation of ship navigation in ice rubble based on peridynamics. Nguyen et al. (2019) introduced a new approach for thermomechanical analysis of shell structures based on peridynamics. Oterkus et. al. (2012) performed impact damage assessment by using peridynamics. Ye et. al. (2017) developed a propeller-ice contact model in peridynamic framework. Zhu et. al. (2016) proposed a new ordinary state-based peridynamic model for polycrystalline materials. In this study, peridynamic fatigue model proposed by Silling and Askari (2014) is utilised to analyse fatigue performance of welded structures. Numerical results are compared with existing experimental results. Finally, the effect of unwelded zone on the fillet welded joint is investigated by simulating the fatigue crack growth in the fillet welded joints.

2 PERIDYNAMIC THEORY

Peridynamic theory is an alternative theory to classical continuum mechanics to overcome limitations of discontinuities, which was proposed by Silling (2000). It is assumed that a body can be represented by material points which occupy a certain volume and interact with other material points within a finite distance called horizon δ through peridynamic bonds. The equation of motion of any material point can be expressed as (Silling and Askari, 2005)

$$\rho(\mathbf{x})\ddot{\mathbf{u}}(\mathbf{x},t) = \int_{H_{\mathbf{x}}} \mathbf{f}(\mathbf{u}(\mathbf{x}',t) - \mathbf{u}(\mathbf{x},t), \mathbf{x}' - \mathbf{x}) dV_{\mathbf{x}'} + \mathbf{b}(\mathbf{x},t) \tag{1}$$

where $H_{\mathbf{x}}$ is the neighbourhood of the material point $\mathbf{x}$ within the horizon δ, ρ is the mass density field, $\mathbf{x}$ is the position vector field, $\mathbf{u}$ is the displacement vector field, t is time, $\mathbf{f}$ is the

pairwise force function which the material point $\mathbf{x}'$ exerts on the material point $\mathbf{x}$, and $\mathbf{b}$ is prescribed body force density field. The interaction of material points in peridynamic theory is shown in Fig. 1.

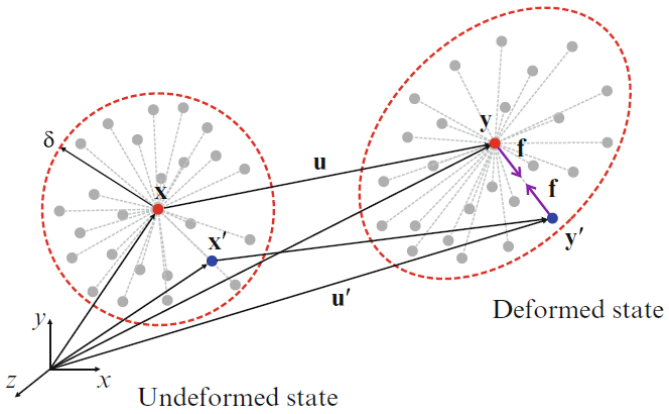

Figure 1. Deformation and interaction of material points $\mathbf{x}$ and $\mathbf{x}'$ (Madenci and Oterkus, 2014)

For a linear elastic material, the pairwise force function is given as

$$\mathbf{f}(\mathbf{u}(\mathbf{x}',t)-\mathbf{u}(\mathbf{x},t),\mathbf{x}'-\mathbf{x})=\frac{\boldsymbol{\xi}+\boldsymbol{\eta}}{|\boldsymbol{\xi}+\boldsymbol{\eta}|}cs \tag{2a}$$

$$\boldsymbol{\xi}=\mathbf{x}'-\mathbf{x} \tag{2b}$$

$$\boldsymbol{\eta}=\mathbf{u}(\mathbf{x}',t)-\mathbf{u}(\mathbf{x},t) \tag{2c}$$

$$s=\frac{|\boldsymbol{\xi}+\boldsymbol{\eta}|-|\boldsymbol{\xi}|}{|\boldsymbol{\xi}|} \tag{2d}$$

where $\boldsymbol{\xi}$ is the relative position between material points $\mathbf{x}$ and $\mathbf{x}'$, $\boldsymbol{\eta}$ is the relative displacement between material points $\mathbf{x}$ and $\mathbf{x}'$, s is the bond stretch, and c is the bond constant. In three-dimensional linear elastic materials, the bond constant can be expressed as

$$c=\frac{18K_B}{\pi\delta^4} \tag{3}$$

where K_B is the bulk modulus and δ is the horizon size.

When the bond stretch is greater than the critical stretch, bond breakage occurs. The critical stretch s_0 is determined by considering the fracture energy, which is the energy that is required to create a unit crack surface. For a linear elastic material, the critical stretch s_0 is expressed as

$$s_0 = \sqrt{\frac{5G_0}{9K_B\delta}} \tag{4}$$

where G_0 is the critical energy release rate. To represent material failure, a history-dependent scalar-valued function μ is defined as

$$\mu = \begin{cases} 1 & if\ s(t', \boldsymbol{\xi}) < s_0 \quad for\ all\ 0 \le t' \le t \\ 0 & otherwise \end{cases} \tag{5}$$

Local damage at a material point is expressed as the ratio of the number of broken bonds to the total number of initially connected bonds to the material point. The local damage φ can be quantified as

$$\varphi(\mathbf{x}, t) = 1 - \frac{\int_{H_\mathbf{x}} \mu(\mathbf{x}, t, \boldsymbol{\xi}) dV_{\mathbf{x}'}}{\int_{H_\mathbf{x}} dV_{\mathbf{x}'}} \tag{6}$$

The range of local damage changes from 0 to 1. When the local damage is 0, all bonds are intact, while the local damage of 1 means that all bonds are broken. Local damage can be used as an indicator of crack formation in the material.

To solve the peridynamic equation of motion given in Eq. (1) numerically, it is necessary to express it in discretized form as

$$\rho_{(k)} \ddot{\mathbf{u}}^n_{(k)} = \sum_{j=1}^{Q} \mathbf{f}\left(\mathbf{u}^n_{(j)} - \mathbf{u}^n_{(k)}, \mathbf{x}_{(j)} - \mathbf{x}_{(k)}\right) V_{(j)} + \mathbf{b}^n_{(k)} \tag{7}$$

where $\rho_{(k)}$ is the mass density of the material point k, n is the n^{th} time step number, Q is the number of material points within the horizon of the material point k, $\mathbf{u}^n_{(k)}$ is the displacement

of the material point k at the n^{th} time step, $V_{(j)}$ is the volume of the material point j, and $\mathbf{b}_{(k)}^{n}$ is the body force density of the material point k at the n^{th} time step.

3 PERIDYNAMIC FATIGUE MODEL

The first peridynamic fatigue model has been proposed by Oterkus et. al. (2010). Their study presented the crack growth of a pre-existing crack by assuming a critical stretch which decreases with cyclic loading. However, their fatigue model was only for crack growth phase. To deal with all phases of fatigue failure, Silling and Askari (2014) has proposed a single peridynamic fatigue model called the "remaining life" consumed by repeated loadings. The developed model can be applied for both phases of crack nucleation and crack growth by using different fatigue parameters in each phase of fatigue failure. This peridynamic fatigue model is a bond-based peridynamic model for a linear elastic material.

3.1 Remaining Life

In peridynamics, local damage in a material is quantified by the number of broken bonds. Bond breakage occurs when the bond stretch between two material points exceeds its critical value. By considering the fatigue behaviour of the material, a concept of remaining life has been introduced by Silling and Askari (2014). This peridynamic fatigue model assumed that the life of a bond connected between two material points is consumed by cyclic loadings. The life reduction ratio of remaining life is determined by

$$\frac{d\lambda_{(k)(j)}}{dN} = -A\left(\varepsilon_{(k)(j)}\right)^{m} \tag{8a}$$

and

$$\lambda_{(k)(j)}^{0} = 1 \tag{8b}$$

where $\lambda_{(k)(j)}$ is the remaining life of bond between material points k and j, N is the number of cycles, A and m are peridynamic fatigue parameters, $\lambda_{(k)(j)}^{0}$ is the remaining life at the initial condition at 0^{th} load cycle and $\varepsilon_{(k)(j)}$ is the cyclic bond strain of the bond between material points k and j. The cyclic bond strain is defined as

$$\varepsilon_{(k)(j)} = \left| s_{(k)(j)}^{+} - s_{(k)(j)}^{-} \right| \tag{9}$$

where $s_{(k)(j)}^{+}$ and $s_{(k)(j)}^{-}$ are the maximum and minimum bond stretches between material points k and j, respectively. They represent two extreme loading conditions in a cycle. For an elastic material, it is assumed that

$$s^{-}_{(k)(j)} = R s^{+}_{(k)(j)} \tag{10}$$

where R is defined as the load ratio. Substituting Eq. (10) into Eq. (9) leads to

$$\varepsilon_{(k)(j)} = \left| s^{+}_{(k)(j)} - s^{-}_{(k)(j)} \right| = \left| (1 - R) s^{+}_{(k)(j)} \right| \tag{11}$$

If a material is subjected to repeated loadings, it is assumed that the cyclic bond strain is independent of number of cycles N and peridynamic fatigue parameters A and m are independent of the position in the material.

Bonds in two different phases are represented in Fig. 2. Bonds near a crack tip within an area are involved in the crack growth phase since they will lead to fatigue crack growth if they are broken, and the other bonds out of this area are involved in the crack nucleation phase. The crack tip area has a size equivalent to the horizon size of material points for pre-existing crack tips.

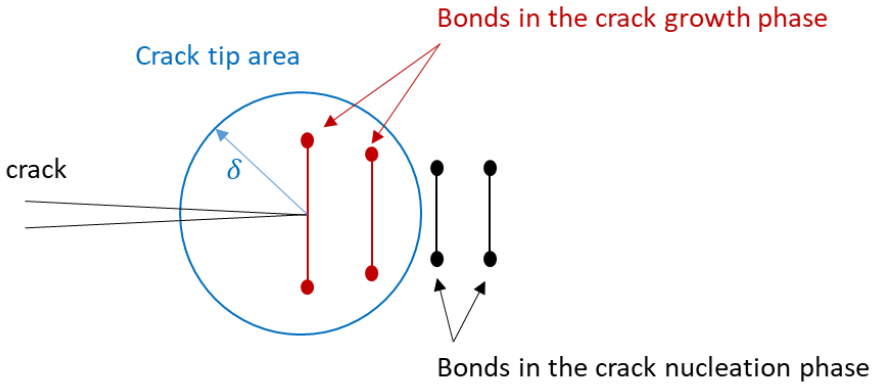

Figure 2. Bonds in two different phases of crack nucleation and crack growth

Note that crack nucleation and fatigue crack growth described by using Eq. (8a) is different than the two-stage crack growth relationship concept described in BS 7910 (2013) and Lukacz (2019).

3.2 Crack Nucleation

Remaining life of each bond in a material inherently has an initial value (Eq. (8b)) and is gradually consumed by cyclic loadings. When the remaining life reaches 0 or is less than 0, bond breakage occurs. Once the bond breaks, it cannot be reconnected.

For the peridynamic fatigue parameters A and m provided in Eq. (8a), the parameters have different values in each phase of fatigue failure, such as crack nucleation and crack growth. The life reduction ratio of bond in the phase of crack nucleation can be described as

$$\frac{d\lambda_{(k)(j)}}{dN} = -A_1\left(\varepsilon_{(k)(j)}\right)^{m_1} \tag{12}$$

where A_1 and m_1 are peridynamic fatigue parameters for crack nucleation. After some mathematical manipulations, Eq. (12) can be represented in logarithmic scale as

$$logN_1 = -logA_1 - m_1 log\varepsilon_1 \tag{13}$$

where ε_1 is the cyclic bond strain of the bond which will break first and $N_1$is the number of cycles for the first bond breakage.

The parameters A_1 and m_1 can be determined by fitting a straight line to experimental data, which is a Strain-Life curve on logarithmic scale as shown in Fig. 3. Strain-Life curve can be expressed in logarithmic scale as

$$logN_f = logC_f - m_f log\Delta\varepsilon \tag{14}$$

where N_f is the number of cycles to failure, $\Delta\varepsilon$ is the strain range, C_f and m_f are constants.

If the fatigue constants C_f and m_f of the strain-life curve for a material are provided, the parameters A_1 and m_1 can be easily obtained by comparing Eq. (13) with Eq. (14). The parameters A_1 and m_1 can be represented as

$$m_1 = m_f \tag{15a}$$

and

$$A_1 = \frac{1}{C_f} \tag{15b}$$

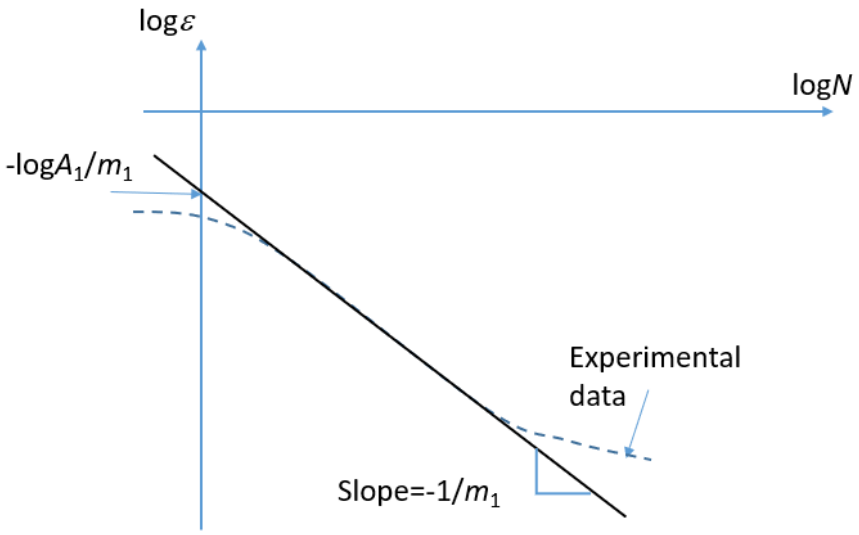

Figure 3. Calibration of peridynamic fatigue parameters A_1 and m_1

3.3 Crack Growth

For a material with a pre-existing crack undergoing repeated loadings, the remaining life of all bonds in the vicinity of a crack tip is calculated by rewriting Eq. (8a) as

$$\frac{d\lambda_{(k)(j)}}{dN} = -A_2\left(\varepsilon_{(k)(j)}\right)^{m_2} \tag{16}$$

where A_2 and m_2 are the peridynamic fatigue parameters for the crack growth phase. The parameters A_2 and m_2 are only valid for bonds within the horizon of the crack tip.

After some mathematical manipulations, Eq. (16) can be written in the form of crack growth rate which can be represented as

$$\frac{da}{dN} = A_2(\bar{\varepsilon}(0))^{m_2} \tag{17}$$

where a is the instantaneous crack length and $\bar{\varepsilon}(0)$ is the cyclic strain of the bond next to crack tip (see Fig. 2).

To predict the fatigue crack growth in structures, the fatigue crack growth rate of many types of materials has been investigated both theoretically and experimentally. The results of tests are compiled into crack growth rate vs. stress intensity factor range curves as shown in Fig. 4. The crack growth rate vs. stress intensity factor range curve is typically divided into three regions. In region 1, there is a threshold of stress intensity factor range ΔK_{th}. If the stress intensity factor range is not greater than this threshold, the crack will not propagate. In region 2, Paris and Erdogan (1963) discovered that the instantaneous crack growth rate is linearly proportional to the stress intensity factor range in the logarithmic scale plot as

$$\frac{da}{dN} = C\Delta K^M \tag{18}$$

where N is the number of cycles, ΔK is the stress intensity factor range, C and M are the fatigue crack growth constants. In region 3, the crack growth is accelerated and when the stress intensity factor reaches the fatigue fracture toughness ΔK_{fc}, final failure will occur.

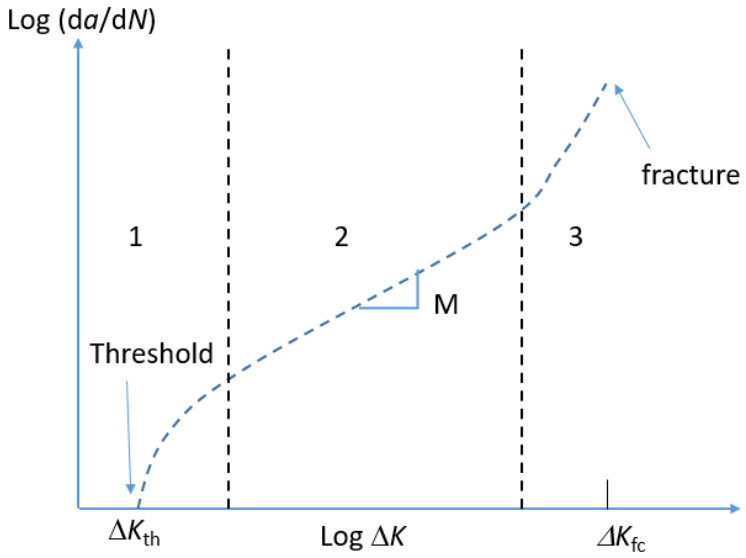

Figure 4. Typical plot of crack growth rate vs. stress intensity factor range in metals

The fatigue parameters C and M can be calibrated from experimental data of crack growth rate vs. stress intensity factor range curve. The parameter m_2 can be determined by comparing Eq. (17) with Eq. (18). Because, $\bar{\varepsilon}(0)$ is proportional to the cyclic stress intensity factor ΔK in Eq. (18), and C and M are constants in Eq. (18), the exponents of Eq. (17) and (18) are same in both expressions as (Silling and Askari, 2014)

$$m_2 = M \tag{19}$$

However, it is more difficult to determine the parameter A_2 since $\bar{\varepsilon}(0)$ in Eq. (17) is an unknown. To determine the parameter A_2, it is first necessary to assign an arbitrary value for the parameter A_2 and then find its actual value by calibrating its value by using crack growth rate vs. stress intensity factor range curve.

4 NUMERICAL RESULTS

In this section, first, numerical results will be presented for fatigue crack growth in ASTM E647 compact tension test made from an aluminium alloy. Then, the fatigue performance of a fillet welded joint will be investigated. All simulations are treated under quasi-static conditions. Also, it is assumed that all material behaviour in peridynamic calculations are linear elastic material behaviour. Quasi-static solutions are obtained by directly assigning zero to inertia terms and solving a matrix system of equations.

4.1. Fatigue Crack Growth in Aluminium Alloys

To validate the peridynamic fatigue model in crack growth phase, the fatigue crack growth is simulated by considering ASTM E647 standard compact tests with a two-dimensional

numerical model for 7075-T651 aluminium alloy. Elastic modulus and Poisson's ratio of 7075-T651 aluminium alloy are specified as 71.7 GPa and 0.33, respectively (Zhao and Jiang, 2008). The geometry of the numerical model is presented in Fig. 5. The numerical model is subjected to a uniaxial tension cyclic load in opposite directions at two pins of top and bottom with extreme forces $P^{+} = 1500$ N and $P^{-} = 150$ N resulting in a load ratio of $R = 0.1$.

Boundary conditions are specified as:

- $u_x = u_y = 0$ at $y = 0$ and $x = 0$

Loading conditions are given as:

- Uniaxial cyclic loading P (MPa) at $x = 50\ mm$ and $y = \pm 14\ mm$

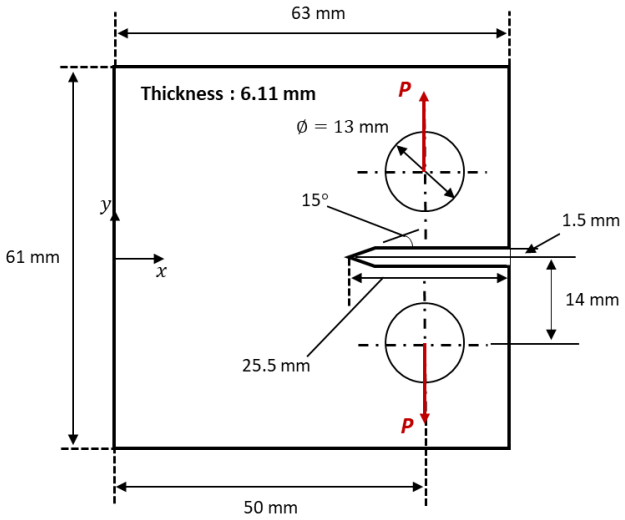

Figure 5. Geometry of numerical model for fatigue crack growth under uniaxial tension cyclic loading

The spacing between material points and the horizon size are specified as 0.5 mm and 1.5075 mm, respectively.

4.1.1 Calibration of Peridynamic Fatigue Parameters for Crack Nucleation

The 7075-T651 aluminium alloy has a special material property called as fatigue limit, which is the minimum threshold causing the fatigue damage (Zhao and Jiang, 2008). If the loading is less than the fatigue limit, regardless of how many loadings are applied, there is no fatigue damage. Incorporating the fatigue limit into the peridynamic fatigue model, Eq. (12) can be modified as (Silling and Askari, 2014)

$$\frac{d\lambda_{(k)(j)}}{dN} = \begin{cases} -A_1\left(\varepsilon_{(k)(j)} - \varepsilon_0\right)^{m_1}, & \text{if } \varepsilon_{(k)(j)} > \varepsilon_0 \\ 0, & \text{otherwise} \end{cases} \tag{20}$$

where $\lambda_{(k)(j)}$ is the remaining life of the bond between material points k and j, N is the number of cycles, A_1 and m_1 are the peridynamic fatigue parameters, $\varepsilon_{(k)(j)}$ is the cyclic bond strain between material points k and j, and ε_0 is the fatigue limit.

To calibrate the parameters A_1 and m_1, fatigue results of Zhao and Jiang (2008) are used to create a Strain-Life curve of 7075-T651 aluminium alloy as shown in Fig. 6. The value of the fatigue limit of 7075-T651 aluminium alloy is also obtained from fatigue test results of Zhao and Jiang (2008). The resulting peridynamic fatigue parameters A_1 and m_1, and the fatigue limit of 7075-T651 aluminium alloy ε_0 are listed in Table 1.

Table 1. Peridynamic fatigue parameters for crack nucleation of 7075-T651

A_1	4824.11
m_1	2.8901
ε_0 (Zhao and Jiang, 2008)	0.0015

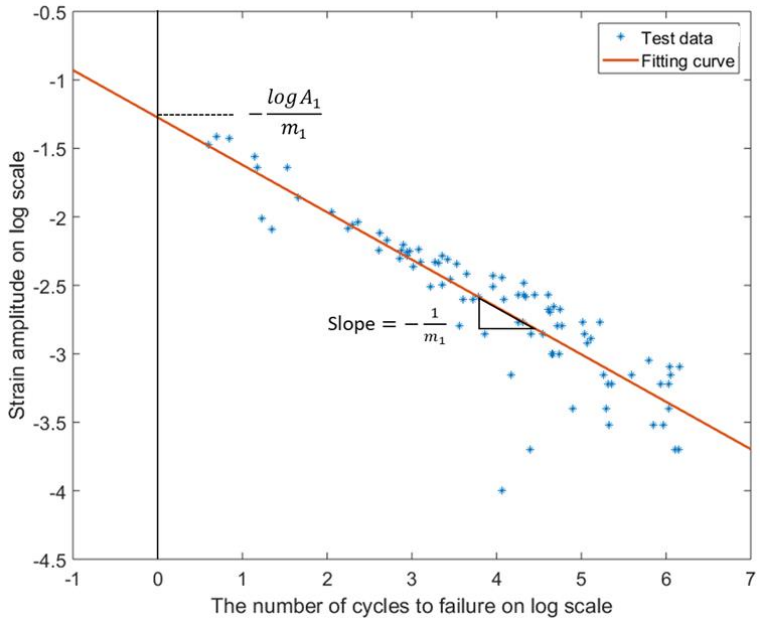

Figure 6. Calibration of peridynamic fatigue parameter A_1 and m_1 in logarithmic scales

4.1.2 Calibration of Peridynamic Fatigue Parameters for Crack Growth

The fatigue crack growth rate of common metallic materials is largely influenced by material microstructure, thickness of the component, and the load ratio (Zhao et. al., 2008). The fatigue crack growth of 7075-T651 aluminium alloy is also significantly influenced by the load ratio. Considering the load ratio effect on the fatigue crack growth rate, Kujawski (2001) proposed the modified Paris law as

$$\frac{da}{dN} = C'(K^*)^{M'} \tag{21a}$$

and

$$K^* = (K_{max})^{\gamma}(\Delta K^+)^{1-\gamma} \tag{21b}$$

where C', M' and γ are the material fatigue constants calibrated by fatigue tests, K_{max} is the maximum stress intensity factor in a loading cycle, and ΔK^+ is the positive part of the range of the stress intensity factor in a loading cycle. These parameters K_{max} and ΔK^+ are presented in Fig. 7.

To consider the load ratio effect in the peridynamic fatigue model, Eq. (16) can be modified by assuming that bond strains near crack tips are proportional to the stress intensity factor, which is written as (Silling and Askari, 2014)

$$\frac{d\lambda_{(k)(j)}}{dN} = -A_2\left(\varepsilon_{(k)(j)}{}^*\right)^{m_2} \tag{22a}$$

and

$$\varepsilon_{(k)(j)}{}^* = \left(\varepsilon_{(k)(j)_{max}}\right)^{\gamma}\left(\Delta\varepsilon_{(k)(j)}{}^+\right)^{1-\gamma} \tag{22b}$$

where γ is the fatigue constant in Eq. (21b), $\varepsilon_{(k)(j)_{max}}$ is the maximum cyclic bond strain between material points k and j at each cycle, and $\Delta\varepsilon_{(k)(j)}{}^+$ is the positive part of the range of cyclic bond strain between material points k and j at each cycle. These parameters $\varepsilon_{(k)(j)_{max}}$ and $\Delta\varepsilon_{(k)(j)}{}^+$ are presented in Fig. 7.

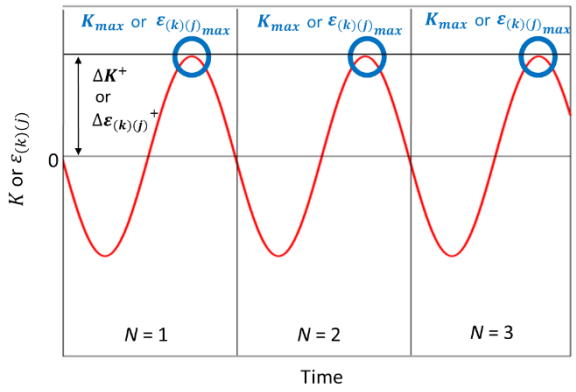

Figure 7. Representation of ΔK^+, K_{max}, $\varepsilon_{(k)(j)_{max}}$ and $\Delta\varepsilon_{(k)(j)}{}^+$ in each load cycle

To calibrate the peridynamic fatigue parameters A_2 and m_2, experimental data (Zhao et. al., 2008) are used to describe the crack growth rate vs. stress intensity factor range curve of 7075-T651 aluminium alloy. In this study, the modified Paris law (Eq. (21a)) is used to consider the load ratio effect. The fatigue constants of 7075-T651 aluminium alloy for Eqs. (21a,b) are presented in Table 2. In this case, the fatigue constants of modified Paris law can be easily obtained from the material properties in Table 2.

The stress intensity factor of the ASTM E647 standard compact specimen can be calculated as (Zhao et. al., 2008)

$$K = \frac{P(2+\frac{a}{W})}{B\sqrt{W}\left(1-\frac{a}{W}\right)^{3/2}}\left(0.886 + 4.64\left(\frac{a}{W}\right) - 13.32\left(\frac{a}{W}\right)^2 + 14.72\left(\frac{a}{W}\right)^3 - 5.6\left(\frac{a}{W}\right)^4\right) \quad (23)$$

where P is the applied force, B is the thickness of the compact specimen, W is the distance between the right edge of the specimen and the vertical line of the applied force P, and a is the length of the crack measured from the line of the applied force P. The crack growth rate of the ASTM E647 standard compact specimen can then be calculated in the analytical way based on Eq. (21a).

Table 2. Fatigue constants of 7075-T651 aluminium alloy (Zhao et. al., 2008)

C'	6.0×10^{-8}
M'	3.32
γ	0.35

The peridynamic fatigue parameter m_2 can be determined from the fatigue constant M' in Eq. (19). The peridynamic fatigue parameter A_2 is determined by using the crack growth rate vs.

crack length curve as shown in Fig. 8. The resulting peridynamic fatigue parameters for crack growth phase are given in Table 3.

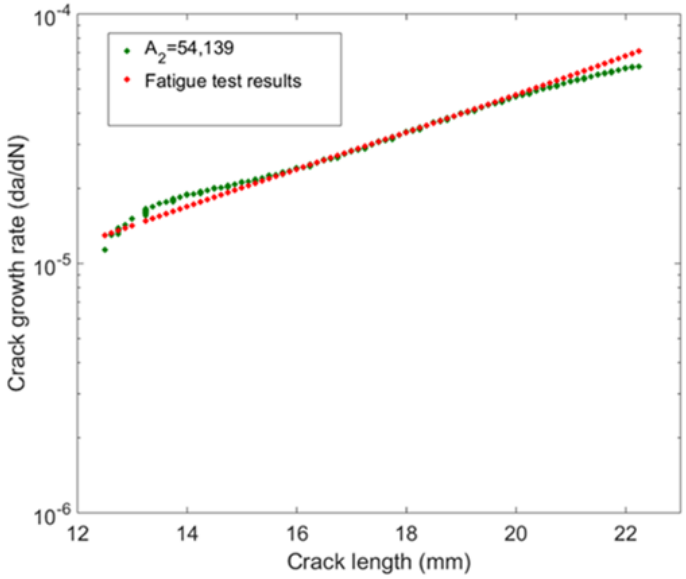

Figure 8. Crack growth rate with respect to crack length for $A_2 = 54139$

Table 3. Peridynamic fatigue parameters for crack growth of 7075-T651

A_2	54138.96
m_2	3.32
γ (Kujawski, 2001)	0.35

4.1.3 Numerical Results and Validation

The fatigue crack growth is demonstrated in Fig. 9, and the fatigue damage is represented as the local damage (Eq. (6)). The numerical result of fatigue crack growth is presented and compared with the fatigue test results of Zhao et. al. (2008) in Fig. 10.

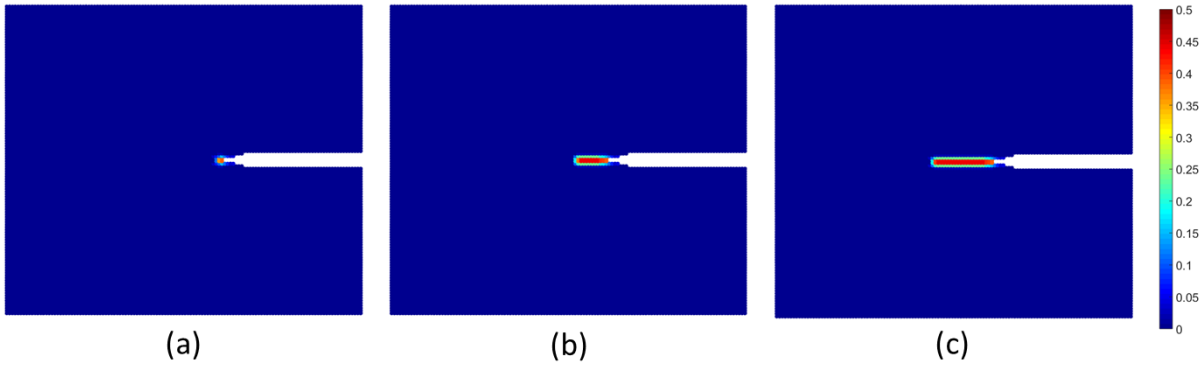

Figure 9. Fatigue damage of numerical results, (a) $N = 0$ and crack length is 12.5 mm, (b) $N = 233706$ and crack length is 17.24 mm, (c) $N = 352196$ and crack length is 22.24 mm

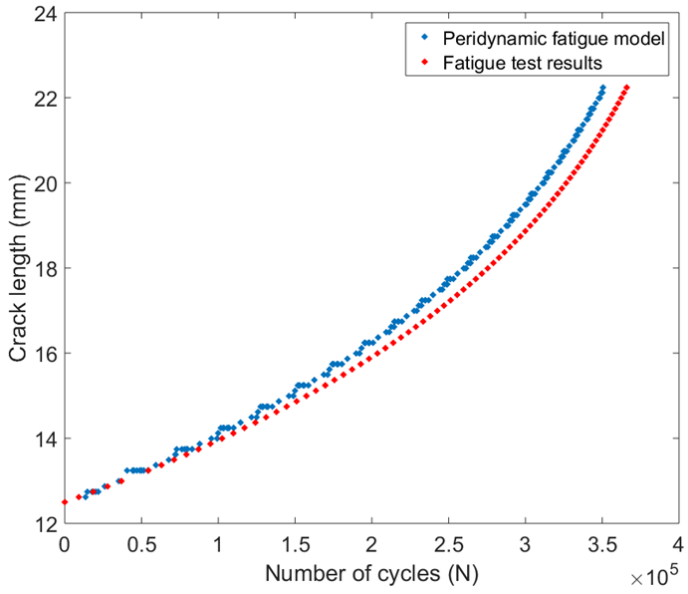

(a)

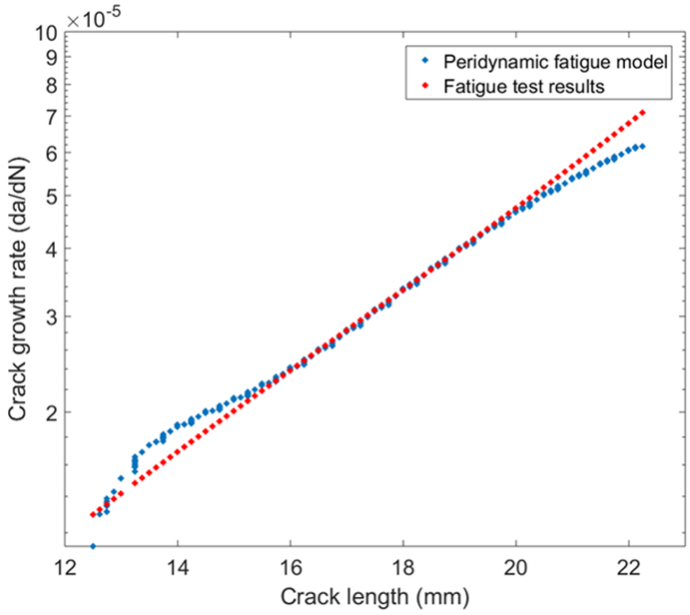

(b)

Figure 10. Numerical results of peridynamic calculation with peridynamic fatigue parameter A_2 and fatigue test results of Zhao et. al. (2008), (a) crack length as a function of number of cycles, (b) crack growth rate as a function of crack length

The numerical results show that the peridynamic fatigue model is capable of predicting the fatigue crack growth. The results of crack length and the crack growth rate from the numerical test agreed well with the fatigue results of Zhao et. al. (2008).

4.2 Fatigue Assessment for Fillet Welded Joints

In this section, a new computational approach to fatigue assessment of fillet welded joints is demonstrated. The effect of unwelded zone in fillet welded joints is investigated by estimating the fatigue performance with respect to the length of unwelded zone. Fatigue failures by crack growth and the path of crack growth in fillet welded joints are simulated by using the peridynamic fatigue model.

4.2.1 Problem Description

A two-dimensional numerical model for fatigue assessment of fillet welded joints is shown in Fig. 11, where $2a$ represents the length of unwelded zone. Two different materials are used in this numerical model. SWS 490B mild carbon steel is used as the material of the main member and AWS A5.18 ER70S-6 is used as the material of the weld metal. The model is subjected to cyclic loading at the top and it is fixed at the bottom. The value of cyclic loading,

σ, is varied from 60 MPa to 100 MPa with a load ratio of 0. Three different length of unwelded zone ($2a$) are considered as 2.4, 4.8 and 7.2 mm.

Boundary conditions are given as:

- $u_y = 0$ at $y = 0$
- $u_x = 0$ at $y = 0$ and $x = 0$

Loading conditions are specified in the form of uniaxial cyclic loading σ (MPa) at $y = 26\ mm$

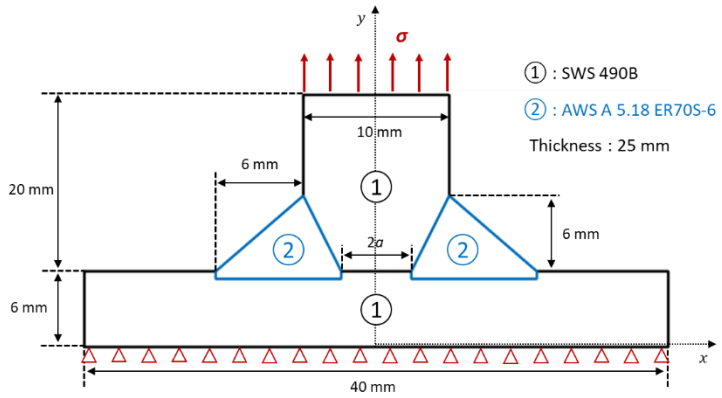

Figure 11. Geometry of a fillet welded joint under uniaxial cyclic loading

4.2.2 Material properties

Elastic modulus and Poisson's ratio of SWS 490B mild carbon steel are specified as 200 GPa and 0.3, respectively (Shim et. al., 2004). For AWS A5.18 ER70S-6, elastic modulus and Poisson's ratio are given as 250 GPa and 0.33, respectively (DeMarte, 2016).

For AWS A5.18 ER70S-6, there are no available fatigue constants for modified Paris law. Therefore, the fatigue constants C', M' and γ are calculated directly in this study. Fatigue constants for AWS A5.18 ER70S-6 are calibrated by using fatigue test results of DeMarte (2016). To calibrate the fatigue constants of modified Paris law C', M' and γ, fatigue test results performed under at least two different load ratio conditions are necessary. The fatigue test results of DeMarte (2016) are presented in Fig. 12 for two different load ratios $R_1 = 0.05$ and $R_2 = 0.6$.

To consider the influence of load ratio it is necessary for all test results of DeMarte (2016) to be converted and expressed into the modified Paris law of Eq. (21a). The fatigue constant γ in Eq. (21b) is determined by the following relation (Kujawski, 2001)

$$\gamma = \frac{log(\Delta K_1^+ / \Delta K_2^+)}{log\left(\frac{1-R_1}{1-R_2}\right)} \tag{24}$$

where R is the load ratio and ΔK^+ is the positive part of the range of the applied stress intensity factor presented in Fig. 7.

Fig. 12 shows calibration for $\Delta K_1{}^+$ and $\Delta K_2{}^+$ of test results of DeMarte (2016). The fatigue constant γ with respect to the crack growth rate can be calculated from Eq. (24).

The modified Paris curve of AWS A5.18 ER70S-6 of Eq. (21a) is presented in Fig. 13. The fatigue constants of the AWS A5.18 ER70S-6 are given in Table 4.

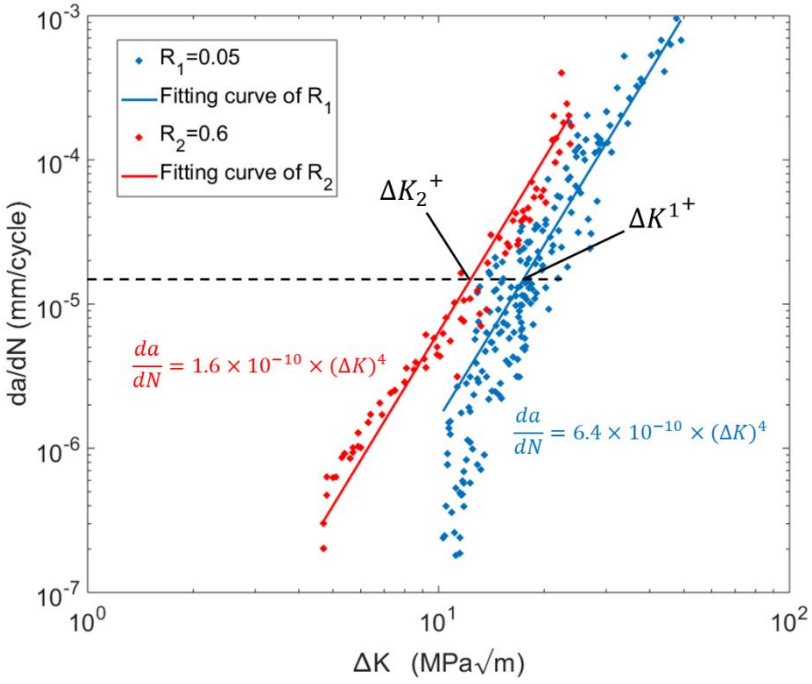

Figure 12. Calibration of $\Delta K_1{}^+$ and $\Delta K_2{}^+$ from test results of DeMarte (2016)

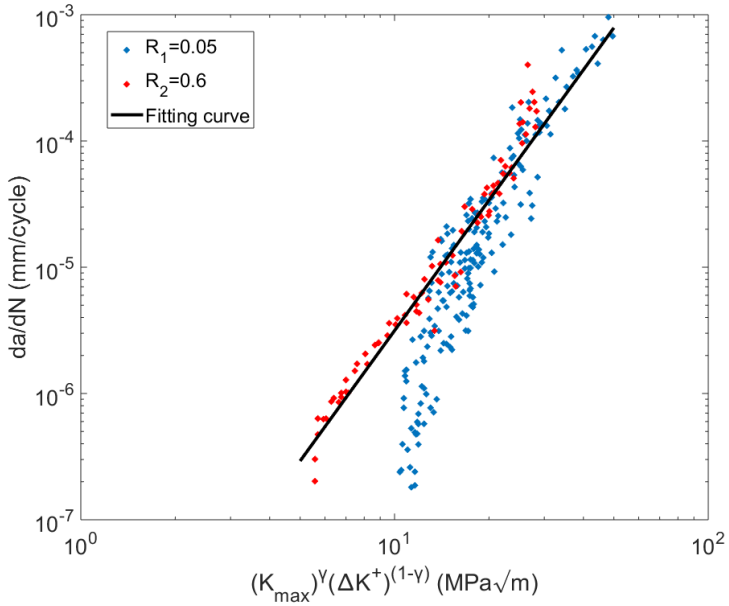

Figure 13. Modified fatigue crack growth data by using test results of DeMarte (2016)

Table 4. Fatigue constants of AWS A5.18 ER70S-6

C'	1.167×10^{-9}
M'	3.43
γ	0.3998

4.2.3 Peridynamic Simulation for Fillet Welded Joints

The thickness of the plate is 25 mm. Spacing between material points and horizon size are specified as 0.2 mm and 0.603 mm, respectively.

It is necessary to calibrate peridynamic fatigue parameters for the simulation of fatigue crack growth in the fillet welded joint. The fillet welded joint involves an unwelded zone, which is considered as a pre-existing crack in the material. Therefore, only peridynamic fatigue parameters A_2 and m_2 of crack growth phase are necessary.

The peridynamic fatigue parameter m_2 can be obtained easily from Eq. (19). For the peridynamic fatigue parameter A_2, a simulation of fatigue crack growth is performed with a two-dimensional numerical model, which is represented in Fig. 14. Two materials are used in the numerical model. One is the ASTM A36 as the main material and the other is the AWS A5.18 ER70S-6 as the weld material. Elastic modulus and Poisson's ratio of ASTM A36 are specified as 200 GPa and 0.33, respectively. The fatigue crack growth in the specimen is demonstrated in Fig. 15, and the result of simulation is compared with the fatigue test results of DeMarte (2016) in Fig. 16. The resulting peridynamic fatigue parameters of AWS A5.18 ER70S-6 are given in Table 5.

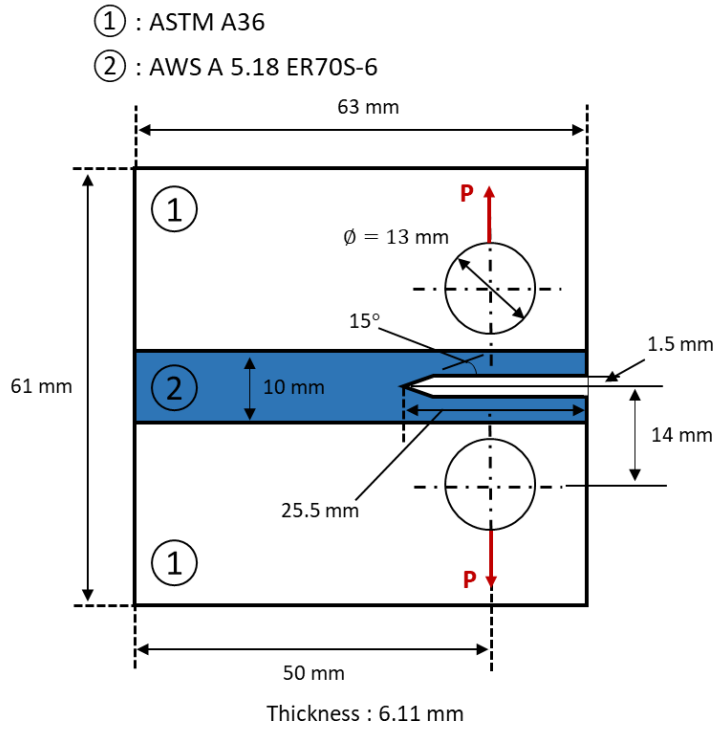

Figure 14. Numerical model for calibration of peridynamic fatigue parameter A_2

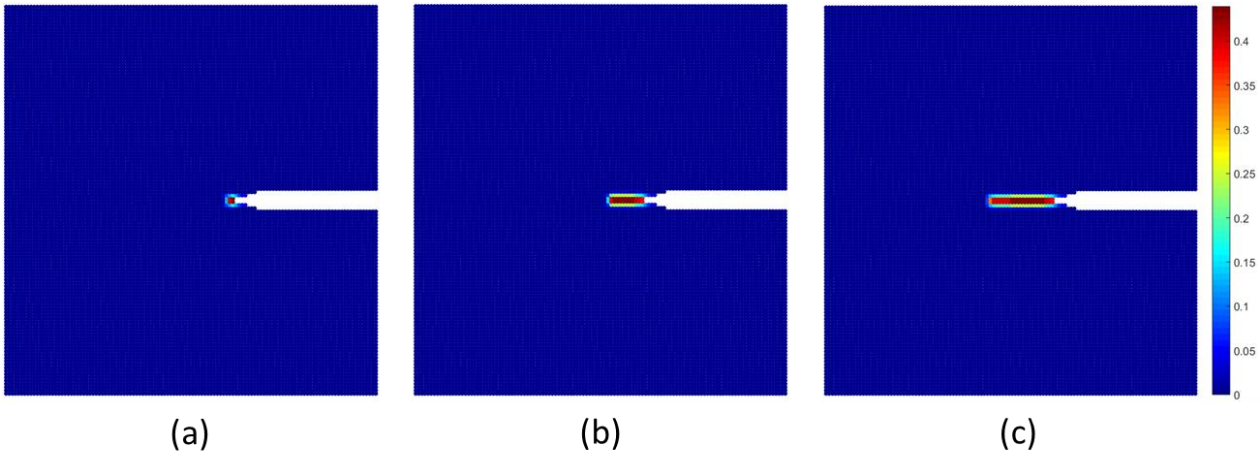

Figure 15. Fatigue damage of numerical results, (a) $N = 0$ and crack length is 12.5 mm, (b) $N = 114{,}915$ and crack length is 17.11 mm, (c) $N = 171{,}468$ and crack length is 22.11 mm

Table 5. Peridynamic fatigue parameters of AWS A5.18 ER70S-6

A_2	1.39×10^5
m_2	3.43
γ	0.3998

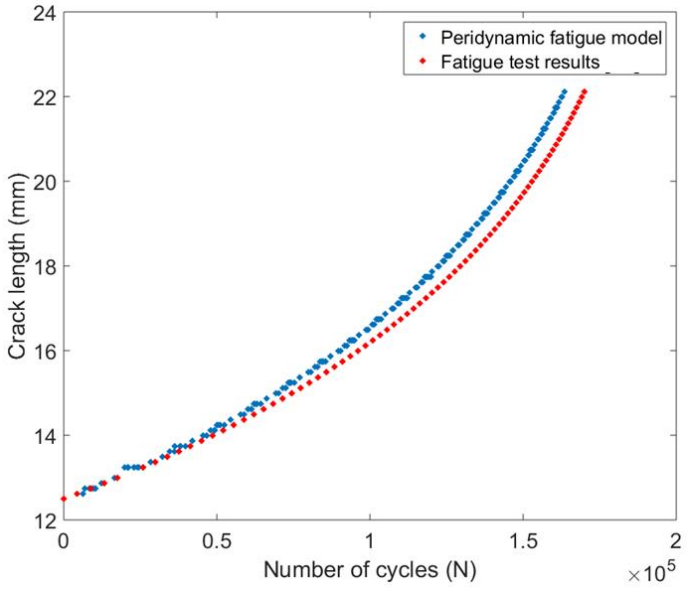

(a)

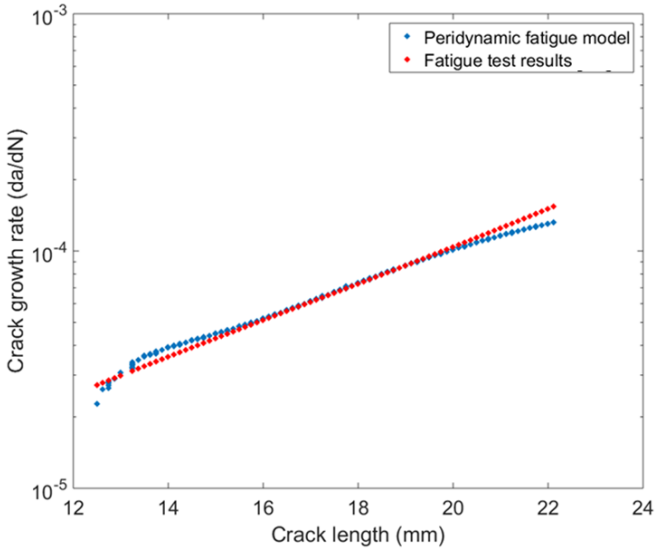

(b)

Figure 16. Numerical results of peridynamic calculation with peridynamic fatigue parameter A_2 and fatigue test results of DeMarte (2016), (a) crack length as a function of number of cycles, (b) crack growth rate as a function of crack length

4.2.4 Numerical Results

After verifying the peridynamic results, peridynamic simulations for fatigue assessment of fillet welded joints are performed. The fatigue crack growth in the fillet welded joint is demonstrated in Fig. 17, 18, and 19, which show the fatigue crack growth in fillet welded joints according to the length of unwelded zones for different conditions. Crack patterns are different

for different length of unwelded zone. However, the crack patterns are similar for same length of unwelded zone even for different loading conditions.

Numerical results of the peridynamic simulations are shown in Fig. 20. The numerical results are fatigue performances of fillet welded joints under different conditions. In Fig. 20, the number of cycles is given when the fillet welded joint model is totally divided into two pieces.

Lee (2010) investigated the characteristics of fatigue failure with respect to the length of unwelded zone. The fatigue tests were performed with the fillet welded joint specimen comprised of the SWS 490B welded with the weld wire of AWS A5.18 ER70S-6 by the GMAW welding method. To validate the numerical results, the results are compared with fatigue test results of Lee (2010) as shown in Figs. 21 and 22.

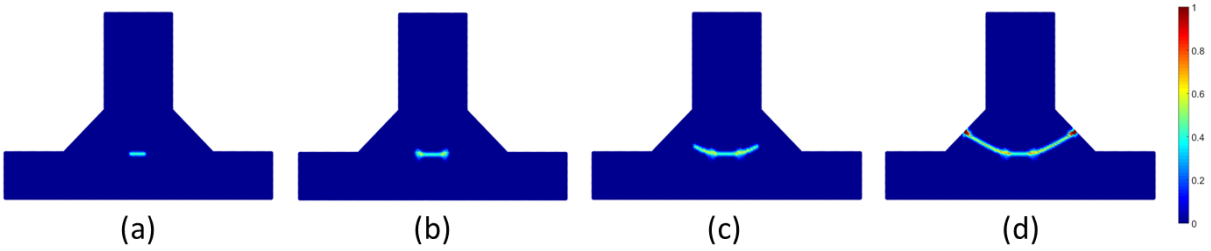

Figure 17. Fatigue damage in numerical model with the length of unwelded zone 2.4 mm for the cyclic loading of σ = 80 MPa (a) $N = 0$ (b) $N = 481{,}468$ (c) $N = 674{,}095$ (d) $N = 699{,}623$

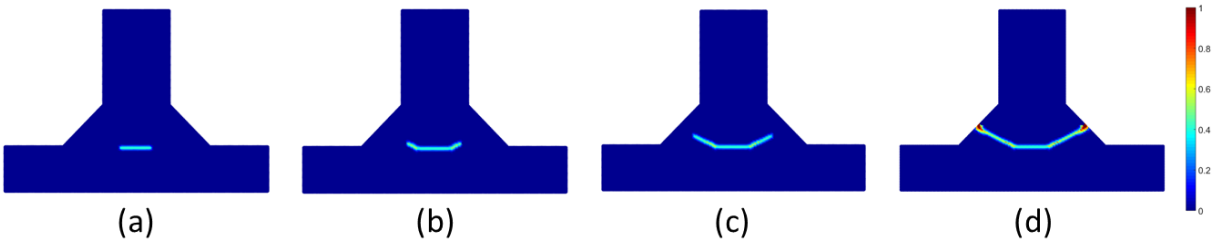

Figure 18. Fatigue damage in numerical model with the length of unwelded zone 4.8 mm for the cyclic loading of σ = 80 MPa, (a) $N = 0$ (b) $N = 183{,}637$ (c) $N = 227{,}882$ (d) $N = 233{,}606$

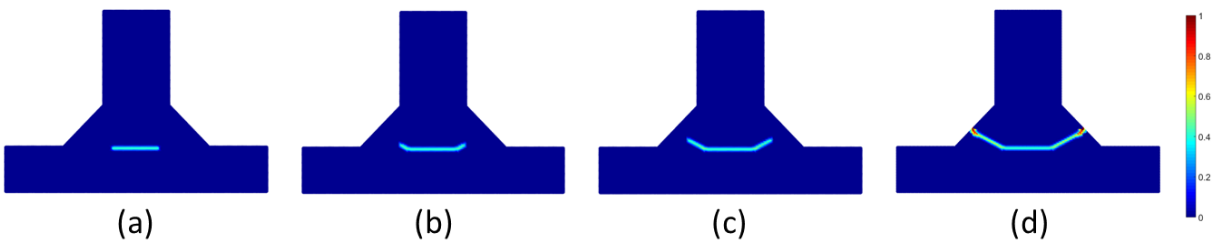

Figure 19. Fatigue damage in numerical model with the length of unwelded zone 7.2 mm for the cyclic loading of σ = 80 MPa, (a) $N = 0$ (b) $N = 74{,}308$ (c) $N = 96{,}210$ (d) $N = 100{,}834$

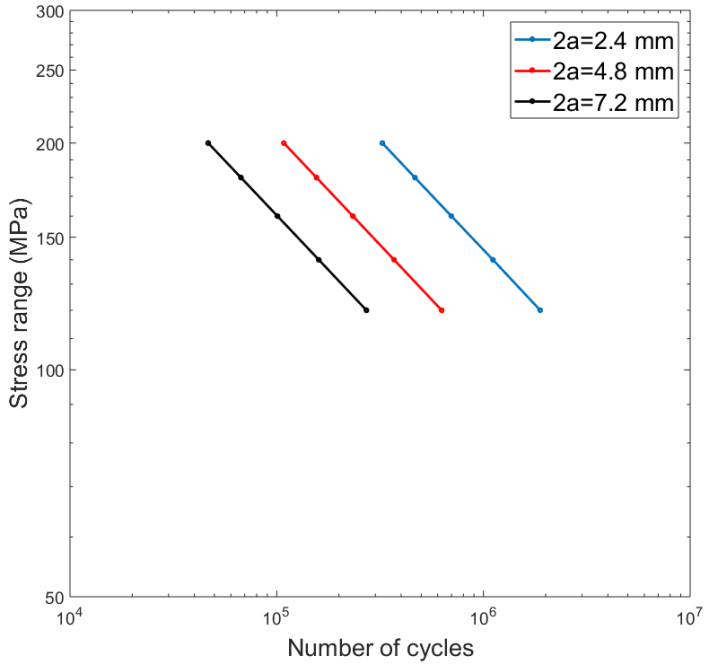

Figure 20. Numerical results of fatigue assessment of fillet welded joints

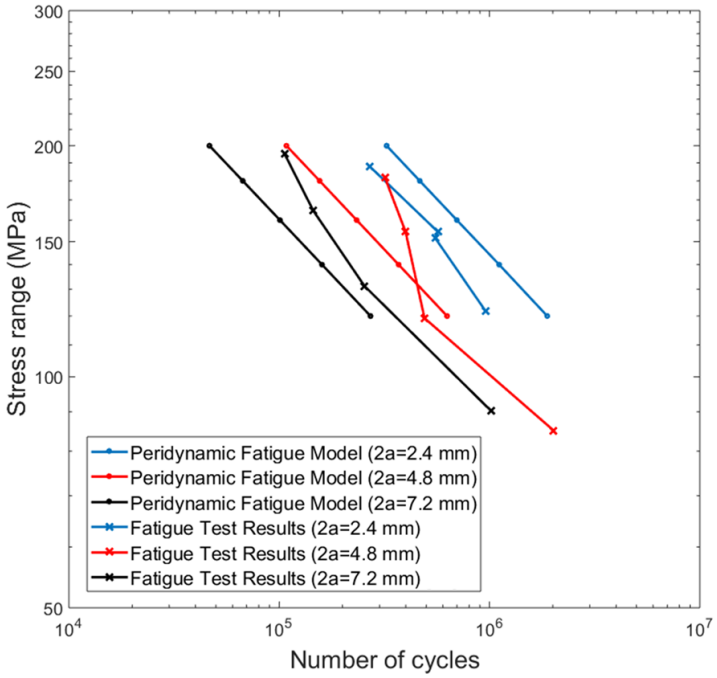

Figure 21. Comparison of fatigue performance of peridynamic simulations with fatigue test results of Lee (2010)

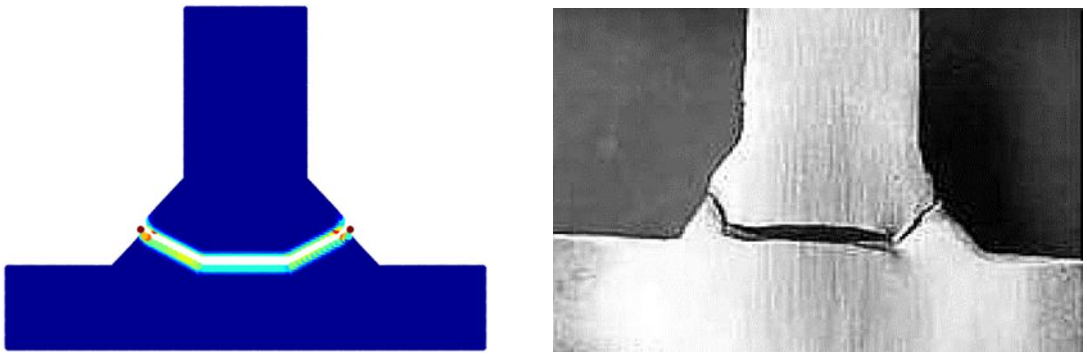

(a) (b)

Figure 22. Fatigue crack growth path with the length of unwelded zone 7.2 mm, (a) peridynamic fatigue model (b) fatigue test result of Lee (2010)

The fatigue crack growth in fillet welded joints according to the length of unwelded zone is simulated by using the peridynamic fatigue model. The numerical results show that the increase in length of unwelded zone decreases the fatigue performance of fillet welded joints. By comparing the numerical results with the fatigue test results of Lee (2010), it is observed that the computational approach with peridynamic fatigue model is capable of estimating the fatigue performance of fillet welded joints. Fig. 21 and 22 show that the results of fatigue performance estimated by peridynamic simulations agreed well with the fatigue results of Lee (2010). Both results show that increasing the length of unwelded zone deteriorates the fatigue performance of fillet welded joints. In addition, the simulation results of fatigue crack growth path in fillet welded joints matched well with the experimental results. The crack initiated at the pre-existing root crack of unwelded zone and propagated to both end of weld material sides. The difference between peridynamic and experimental results in Fig. 21 may be related to the assumptions made in the numerical model since it is assumed that the materials are elastic and 2-Dimensional model is utilised. Overall, it is confirmed that the peridynamic fatigue model can be used to simulate the actual behaviour of fatigue crack growth for welded joints.

5 CONCLUSION

In this study, the fatigue crack growth in fillet welded joints was investigated by using peridynamic fatigue model and the fatigue performance was estimated by considering the weld geometry effect of the unwelded zone. The peridynamic fatigue model in the fatigue crack growth phase was validated by numerical compact tests with two-dimensional ASTM E647 standard compact specimens under tension loading. The results of peridynamic fatigue model were compared with the fatigue test results of Zhao et. al. (2008). Numerical results showed that the peridynamic fatigue model is capable of predicting the fatigue crack growth. Next, the

fatigue crack growth in fillet welded joints was analysed according to the length of unwelded zone. The numerical results showed that the increase in the length of the unwelded zone in fillet welded joints decreases the fatigue performance. Also, by comparing the numerical results with the fatigue test results of Lee (2010), it is confirmed that the computational approach with peridynamic fatigue model is capable of estimating the fatigue performance of fillet welded joints.

REFERENCES

Alpay, S. and Madenci, E., 2013. Crack growth prediction in fully-coupled thermal and deformation fields using peridynamic theory. In *54th AIAA/ASME/ASCE/AHS/ASC structures, structural dynamics, and materials conference* (p. 1477).

Barsoum, Z., & Jonsson, B., 2011. Influence of weld quality on the fatigue strength in seam welds. *Engineering Failure Analysis*, *18*(3), 971-979.

Basoglu, M.F., Zerin, Z., Kefal, A. and Oterkus, E., 2019. A computational model of peridynamic theory for deflecting behavior of crack propagation with micro-cracks. *Computational Materials Science*, *162*, pp.33-46.

Bie, Y.H., Liu, Z.M., Yang, H. and Cui, X.Y., 2020. Abaqus implementation of dual peridynamics for brittle fracture. *Computer Methods in Applied Mechanics and Engineering*, *372*, p.113398.

BS 7910 k, 2013. Guide to Methods for Assessing the Acceptability of Flaws in Metallic Structures, 2013 + A1:2015.

Chen, W., Gu, X., Zhang, Q. and Xia, X., 2020. A refined thermo-mechanical fully coupled peridynamics with application to concrete cracking. *Engineering Fracture Mechanics*, p.107463.

Coughlin, R. and Walbridge, S., 2012. Fatigue testing and analysis of aluminum welds under in-service highway bridge loading conditions. *Journal of Bridge Engineering*, *17*(3), pp.409-419.

DeMarte, R. A., 2016. Analysis of Fatigue Crack Propagation in Welded Steels.

Dong, Y., Su, C. and Qiao, P., 2020. An improved mesoscale damage model for quasi-brittle fracture analysis of concrete with ordinary state-based peridynamics. *Theoretical and Applied Fracture Mechanics*, p.102829.

Gravouil, A., Moës, N., & Belytschko, T., 2002. Non-planar 3D crack growth by the extended finite element and level sets—Part II: Level set update. *International Journal for Numerical Methods in Engineering*, *53*(11), 2569-2586.

Huang, Y., Oterkus, S., Hou, H., Oterkus, E., Wei, Z. and Zhang, S., 2019. Peridynamic model for visco-hyperelastic material deformation in different strain rates. *Continuum Mechanics and Thermodynamics*, pp.1-35.

Imachi, M., Tanaka, S., Bui, T.Q., Oterkus, S. and Oterkus, E., 2019. A computational approach based on ordinary state-based peridynamics with new transition bond for dynamic fracture analysis. *Engineering Fracture Mechanics*, *206*, pp.359-374.

Imachi, M., Tanaka, S., Ozdemir, M., Bui, T.Q., Oterkus, S. and Oterkus, E., 2020. Dynamic crack arrest analysis by ordinary state-based peridynamics. *International Journal of Fracture*, *221*(2), pp.155-169.

Kujawski, D., 2001. A fatigue crack driving force parameter with load ratio effects. *International Journal of Fatigue, 23*, 239-246.

Lee, Y. B., 2010. Characteristics of Fatigue Failure according to Thickness of Material and Number of Passes in Cruciform Fillet Weld Zone. *Journal of Welding and Joining, 28*(6), 45-50.

Liu, R.W., Xue, Y.Z., Lu, X.K. and Cheng, W.X., 2018. Simulation of ship navigation in ice rubble based on peridynamics. *Ocean Engineering*, *148*, pp.286-298.

Lukács, J., Meilinger, Á. and Pósalaky, D., 2018. High cycle fatigue and fatigue crack propagation design curves for 5754-H22 and 6082-T6 aluminium alloys and their friction stir welded joints. *Welding in the World*, *62*(4), pp.737-749.

Lukács, J., 2019. Fatigue crack propagation limit curves for high strength steels based on two-stage relationship. *Engineering Failure Analysis*, *103*, pp.431-442.

Maddox, S.J., 2003. Review of fatigue assessment procedures for welded aluminium structures. *International Journal of Fatigue, 25*(12), pp.1359-1378.

Madenci, E., & Oterkus, E. (2014). Peridynamic theory and its applications. Springer.

Moës, N., Gravouil, A., & Belytschko, T., 2002. Non-planar 3D crack growth by the extended finite element and level sets—Part I: Mechanical model. *International Journal for Numerical Methods in Engineering, 53*(11), 2549-2568.

Nguyen, C.T. and Oterkus, S., 2019. Peridynamics for the thermomechanical behavior of shell structures. *Engineering Fracture Mechanics*, *219*, p.106623.

Nguyen, O., Repetto, E. A., Ortiz, M., & Radovitzky, R. A., 2001. A cohesive model of fatigue crack growth. *International Journal of Fracture, 110*(4), 351-369.

Ortiz, M., & Pandolfi, A., 1999. Finite-deformation irreversible cohesive elements for three-dimensional crack-propagation analysis. *International journal for numerical methods in engineering, 44*(9), 1267-1282.

Oterkus, E., Guven, I., & Madenci, E., 2010. Fatigue failure model with peridynamic theory. In Thermal and Thermomechanical Phenomena in Electronic Systems (ITherm), 2010 12th IEEE Intersociety Conference on (pp. 1-6). IEEE.

Oterkus, E., Guven, I. and Madenci, E., 2012. Impact damage assessment by using peridynamic theory. *Open Engineering*, *2*(4), pp.523-531.

Oterkus, S., Madenci, E., & Agwai, A. (2014). Peridynamic thermal diffusion. *Journal of Computational Physics, 265*, 71-96.

Paris, P., & Erdogan, F., 1963. A critical analysis of crack propagation laws. *Journal of Basic Engineering, 85*(4), 528-533.

Rozumek, D., Lewandowski, J., Lesiuk, G. and Correia, J.A., 2020. The influence of heat treatment on the behavior of fatigue crack growth in welded joints made of S355 under bending loading. *International Journal of Fatigue, 131*, p.105328.

Shim, J. S., Kim, C. H., & Kim, D. J., 2004. 3D Finite Element Analysis of High Tension Bolted Joints. *Journal of Korean society of steel construction, Korean society of steel construction, 16*(4), 407-413.

Silling, S.A., 2000. Reformulation of elasticity theory for discontinuities and long-range forces. *Journal of the Mechanics and Physics of Solids*, *48*(1), pp.175-209.

Silling, S. A., & Askari, E., 2005. A meshfree method based on the peridynamic model of solid mechanics. *Computers & structures, 83*(17-18), 1526-1535.

Silling, S. A., & Askari, A., 2014. Peridynamic model for fatigue cracking. SAND2014-18590. Albuquerque: Sandia National Laboratories.

Sonsino, C. M., 2009. Effect of residual stresses on the fatigue behaviour of welded joints depending on loading conditions and weld geometry. *International Journal of Fatigue, 31*(1), 88-101.

Teng, T. L., Fung, C. P., & Chang, P. H., 2002. Effect of weld geometry and residual stresses on fatigue in butt-welded joints. *International journal of pressure vessels and piping, 79*(7), 467-482.

Vazic, B., Wang, H., Diyaroglu, C., Oterkus, S. and Oterkus, E., 2017. Dynamic propagation of a macrocrack interacting with parallel small cracks. *AIMS Materials Science*, *4*(1), pp.118-136.

Vazic, B., Oterkus, E. and Oterkus, S., 2020. Peridynamic model for a Mindlin plate resting on a Winkler elastic foundation. *Journal of Peridynamics and Nonlocal Modeling*, pp.1-10.

Ye, L.Y., Wang, C., Chang, X. and Zhang, H.Y., 2017. Propeller-ice contact modeling with peridynamics. *Ocean Engineering*, *139*, pp.54-64.

Zaccariotto, M., Luongo, F., & Galvanetto, U., 2015. Examples of applications of the peridynamic theory to the solution of static equilibrium problems. *The Aeronautical Journal, 119*(1216), 677-700.

Zhao, T., & Jiang, Y., 2008. Fatigue of 7075-T651 aluminum alloy. *International Journal of Fatigue, 30*(5), 834-849.

Zhao, T., Zhang, J., & Jiang, Y., 2008. A study of fatigue crack growth of 7075-T651 aluminum alloy. *International Journal of Fatigue, 30*(7), 1169-1180.

Zhu, N., De Meo, D. and Oterkus, E., 2016. Modelling of granular fracture in polycrystalline materials using ordinary state-based peridynamics. *Materials*, *9*(12), p.977.

Zi, G., & Belytschko, T. (2003). New crack-tip elements for XFEM and applications to cohesive cracks. International Journal for Numerical Methods in Engineering, 57(15), 2221-2240.